A high-resistivity phase induced by swift heavy-ion irradiation of Bi: a probe for thermal spike damage?

1993 J. Phys.: Condens. Matter 5 4573

(http://iopscience.iop.org/0953-8984/5/26/027)

J. Phys.: Condens. Matter 5 (1993) 4573–4584. Printed in the UK

A high-resistivity phase induced by swift heavy-ion irradiation of Bi: a probe for thermal spike damage?

C Dufour†, A Audouard‡, F Beuneu§, J Dural†, J P Girard¶, A Hairie¶, M Levalois¶, E Paumier†¶ and M Toulemonde†

† CIRIL, Laboratoire mixte CEA–CNRS, rue Claude Bloch, BP 5133, 14040 Caen, France
‡ Laboratoire de Physique des Solides et Service National des Champs Magnétiques Pulsés, Complexe Scientifique de Rangueil, 31077 Toulouse, France
§ LSI Ecole Polytechnique, Rte de Saclay, 91128 Palaiseau, France
¶ LERMAT, URA CNRS 1317, ISMRA, 6 Boulevard du Maréchal Juin, 14050 Caen, France

Received 4 January 1993, in final form 6 April 1993

Abstract. Pure bismuth samples were irradiated at 20 K with swift heavy ions from ^{18}O to ^{238}U in the GeV range. The rate of the induced damage was deduced from *in situ* electrical resistance measurements. Above a threshold in the electronic stopping power S_e equal to 24 keV nm^{-1}, the damage is due to electronic slowing down. Above 30 keV nm^{-1}, the electronic slowing down is efficient enough to induce latent tracks attributed to the appearance of a high-resistivity phase. The induced latent tracks radii can be up to 21.9 nm for $S_e = 51$ keV nm^{-1} which is the largest value reported so far for non-radiolytic materials. The evolution with S_e of the latent tracks radii is calculated on the basis of the thermal spike model, assuming a realistic value for the electron–phonon coupling constant. A rather good agreement is obtained which supports the idea that the thermal spike could be operative in the observed radiation damage.

1. Introduction

In the last decade, the availability of swift heavy-ion facilities has allowed numerous irradiation experiments in the electronic slowing down regime. These experiments have demonstrated that the electronic slowing down is able to induce atomic movements not only, as expected, in insulators [1] but also in metallic systems [2–9]. However, the basic question which remains to be answered concerns the mechanism by which the ion energy is transferred to the lattice atoms. Two models have been proposed to account for the experimental data: the thermal spike model [10–12] and the ionic spike model [9, 13]. The aim of the present paper is to decide whether or not the energy transferred to the host electrons can induce significant atomic motion through the electron–phonon (E–P) interaction. Indeed, several experimental works suggest that E–P coupling might be a key parameter for the observed effects. For example, it has been shown [6] that the amount of electronic slowing down required to induce damage in amorphous Ni–B alloy is lower than for its crystalline counterpart, and it is thought that for a given composition the E–P coupling is stronger in amorphous than in crystalline alloys; besides, amorphous alloys are extremely sensitive to radiation damage in the electronic slowing down regime [2, 3]. On the other hand, no electronic slowing down effect is observed in crystalline noble metals such as Ag and Cu for which the E–P coupling is weak [7, 14] whereas pure metals which are sensitive to swift heavy-ion irradiation exhibit soft-phonon modes and strong E–P coupling [7, 15, 16].

In the framework of the thermal spike model, Seitz and Koehler [11] predict that the lattice temperature in the core of an ion track can reach 500 K in noble metals whereas in

0953-8984/93/264573+12$07.50

transition metals with a strong E–P coupling the core temperature may reach up to 5×10^4 K. This result is in agreement with the idea that compounds with strong E–P coupling are susceptible to exhibit electronic-slowing-down-induced latent tracks. The thermal spike model has been extended to allow latent track radii calculations [17–21], based on the theoretical considerations made by Kaganov *et al* [22] and Allen [23] for the strength of the E–P coupling, and by Martynenko and Yavlinskii [24] for the diffusivity of hot electrons. Using realistic values for the E–P coupling [17], the calculated radii of cylinders of matter melted and rapidly quenched along the ion path were in good agreement with the latent track radii either directly observed by transmission electron microscopy in a-Si and a-Ge [25] or deduced from a phenomenological model in a-$Fe_{85}B_{15}$ [26].

Assuming, as suggested above, that the thermal spike is a dominant mechanism for the irradiation damage induced by electronic slowing down, the largest effects should be expected in materials which exhibit (i) strong E–P coupling, (ii) low melting temperature and (iii) specific volume larger in the solid than in the liquid phase, in order to avoid any inhibition of the melting due to compressive stresses. This is the case of bismuth which, in addition, can be amorphized by vapour deposition on cold substrate [27, 28]. It is worthwhile to notice that, when a 40 nm thick amorphous bismuth film, vapour deposited at 4 K, is annealed at a rate of 5 K min^{-1}, a crystalline phase starts to appear at a temperature of 10 K. At 20 K, crystallization is achieved and the resistivity of the recrystallized phase (of the order of 1500 $\mu\Omega$ cm at 20 K [27, 28]) is much higher than the resistivity of both bulk Bi (7 $\mu\Omega$ cm, see table 1) and amorphous Bi films (100 $\mu\Omega$ cm). Moreover this high-resistivity phase is stable up to 85 K [28]. Another striking difference between the as-deposited and the annealed phase lies in the superconducting properties: while the amorphous phase exhibits a superconducting transition at 6 K the annealed phase remains in the normal state down to 4 K. As will be seen in section 3 this set of peculiar properties can be used as a probe for the radiation damage. Moreover, the radiation damage of bismuth in the nuclear stopping power regime has been widely studied [29–33]. In particular, electron irradiation experiments have allowed the measurement of the threshold displacement energy (T_d = 13 eV) and the Frenkel pair resistivity (ρ_{FP} = 0.6 Ω cm) [32]. The saturation resistivity is of the order of 400 $\mu\Omega$ cm and the spontaneous recombination volume lies between 100 and 200 atomic volumes [32, 33]. It must be pointed out that, due to the semi-metallic character of bismuth, the radiation damage occurs in two steps. Indeed, in the first step, the defects created by nuclear collisions act as donors, compensating holes which are dominant carriers in non-irradiated pure Bi. The measured resistivity increment is then due first to the decrease of both the carrier density and mobility. In the second step, after hole compensation, the resistivity increment is due only to the reduction in carrier mean free path as usual in irradiated crystalline metals. The data obtained from both the 5 MeV α-particle [34] and fast-neutron irradiations [35] are in overall agreement with the results of electron irradiation.

2. Experimental details

The samples were prepared from pure bismuth by melting and subsequent casting under a controlled atmosphere. Polycrystalline ingots were annealed and cut with a wire saw in the form of ribbons, typically 0.5 mm wide and 1 cm long. The samples were then chemically thinned down to 50 μm and, finally, four platinum or gold wires 20 or 50 μm in diameter were soldered on the ribbon surface in order to perform conventional four-point resistance measurements. The residual resistivity ratio $\rho_{300\ K}/\rho_{10\ K}$ ranged from 6 to 28 (table 1) as expected for pure bismuth [36].

Table 1. Experimental conditions. (1) Ion beam: mass and energy. (2) R_p projected range [38]. (3) Thickness of the samples, resistivity at 10 K (ρ(10 K)) and the resistivity ratio between 300 K and 10 K. (4) S_e or dE/dx electronic energy deposition, σ_N nuclear collisions cross section. (5) $d\Delta\rho/d\phi t$ at $\phi t = 0$ for each sample and the resistivity per defect (ρ_d). (6) ρ_d/ρ_{PF} ratio between ρ_d and the Frenkel-pair resistivity.

Ion	Incident Energy (MeV/amu)	Range R_p (μm)	Thickness (μm)	ρ(10 K) (Ω cm)	$\frac{\rho(300\text{ K})}{\rho(10\text{ K})}$	dE/dx (keV nm^{-1})	σ_N (cm^2)	$d\Delta\rho/d\phi t$ at $\phi t = 0$ (Ω cm^3/ions)	ρ_d (Ω cm)	ρ_d/ρ_{PF} †
^{18}O	10.5	120	56	5.6×10^{-6}	21	1.2	6.1×10^{-18}	2.5×10^{-18}	0.41	0.68
^{24}Mg	11	90	45	5.9×10^{-6}	21	2.6	9.6×10^{-18}	3.3×10^{-18}	0.34	0.53
^{86}Kr	58	520	60	6.3×10^{-6}	20	6.5	1.8×10^{-17}	7.9×10^{-18}	0.43	0.74
	25	170	75	8.2×10^{-6}	21	12	4.6×10^{-17}	1.7×10^{-17}	0.38	0.63
^{129}Xe	39.6	245	50	7.3×10^{-6}	16	17	5.5×10^{-17}	1.7×10^{-17}	0.31	0.51
	19.1	100	70	29×10^{-6}	6.5	25	1.6×10^{-16}	1.2×10^{-16}	0.75	1.3
^{181}Ta	31.4	170	70	12×10^{-6}	12.5	32	1.1×10^{-16}	1.9×10^{-16}	1.7	2.8
	31.4	170	50	9.1×10^{-6}	16	32	1.0×10^{-16}	1.9×10^{-16}	1.9	3.2
	19.7	105	50	3.9×10^{-6}	22	37	1.9×10^{-16}	3.0×10^{-15}	16	27
	18.8	100	58	4.2×10^{-6}	28	38	2.3×10^{-16}	6.1×10^{-15}	27	45
	18.8	100	52	7.2×10^{-6}	16	38	2.2×10^{-16}	4.8×10^{-15}	22	37
^{208}Pb	19.2	100	60	9.5×10^{-6}	13	44	2.7×10^{-16}	1.6×10^{-14}	59	98
^{238}U	14.5	80	58	7.5×10^{-6}	16	49	5.7×10^{-16}	2.7×10^{-14}	47	78
	14.5	80	52	7.9×10^{-6}	15	50	5.0×10^{-16}	3.7×10^{-14}	74	123
	14.5	80	52	8.2×10^{-6}	13	50	5.0×10^{-16}	3.6×10^{-14}	72	120
	14.5	80	42	8.5×10^{-6}	11	51	4.2×10^{-16}	3.9×10^{-14}	94	157

† the resistivity of a Frenkel pair in Bi $\rho_{PF} = 0.6\ \Omega$ cm [32].

Heavy-ion irradiations (from ^{18}O to ^{238}U) were performed at GANIL either in the IRABAT [37] or the IRASME [37] facilities. Table 1 summarizes the experimental conditions, in particular the electronic stopping powers which ranged from 1.2 to 51 keV nm^{-1} as given by TRIM [38]. When the ion projected range was large enough (Kr, Xe, Ta), two samples separated by an aluminium or copper foil degrader were irradiated so that two values of S_e were investigated. In all cases, the total sample thickness was kept smaller than the ion projected range. Irradiations were performed in cold (10 K) helium gas at normal pressure and the flux was limited to avoid any temperature larger than 20 K.

The sample resistance was measured *in situ* as a function of the ion fluence. After the irradiation 10 minute isochronal annealings were performed with resistance measurements *in situ*.

3. Results and analysis

Figures 1 and 2 show the variation of resistivity $\Delta\rho$ as a function of the ion fluence Φt for 0.189 GeV ^{18}O, and 3.99 GeV ^{208}Pb ions respectively. The influence of the electronic slowing down [38] on irradiation damage is demonstrated in figure 3 where $\rho_d = (d\Delta\rho/d\Phi t)_0/\sigma_N$ in which $(d\Delta\rho/d\Phi t)_0$ is the initial damage rate and σ_N the nuclear collision cross section [38, 39] is plotted as a function of the electronic energy loss S_e. Three S_e regimes can be distinguished in the figure:

(i) for S_e less than 20 keV nm^{-1}, ρ_d is lower than in the case of electron irradiation [32] for which $\rho_d = 0.6\ \Omega$ cm. Such behaviour may be due to intra-cascade recombination of vacancies and interstitials as in copper [43] or to defect annealing by electronic excitations as in nickel [4], or iron at low S_e [5]. Whatever the irradiation-induced annealing mechanism, the defect creation can be attributed to nuclear collisions in this S_e regime which will be called the 'nuclear collision regime' in the following.

(ii) for S_e ranging from 20 to 30 keV nm^{-1}, ρ_d is an increasing function of S_e which is the signature of a growing contribution of the electronic slowing down to the irradiation damage. This S_e range will be referred in the following as the 'threshold regime'. It must be noted that the S_e threshold value (24 keV nm^{-1}), although higher than in amorphous $Fe_{85}B_{15}$ ($\simeq$ 10 keV nm^{-1} [3]), is lower than in crystalline iron (40 keV nm^{-1} [5]) and crystalline Ni_3B (30 keV nm^{-1} [6]).

(iii) for S_e higher than 30 keV nm^{-1}, ρ_d saturates towards a very high value, of the order of 100 Ω cm dpa^{-1}, i.e. about 160 times higher than for electron irradiation. This regime will be called the 'electronic regime' in the following.

All experimental data have been analysed using the phenomenological equation:

$$\Delta\rho = \Delta\rho_s[1 - \exp(-\sigma\Phi t)] \tag{1}$$

where $\Delta\rho_s$ is the saturation resistivity increment and σ is a cross section. As it will be seen, the physical meaning of those parameters depends on the damage mechanism.

In the nuclear collision regime, only the high-fluence part of the damage curve can be accounted for by (1) as can be seen in figure 1, where the solid line fits (1). Such behaviour can be interpreted on the basis of the two-step damage process mentioned in the introduction: at low fluence, the damage is due to the decrease in both the carrier concentration and the mean free path while at higher fluence, the damage is only due to the decrease in the mean free path. In the framework of the recombination volume model

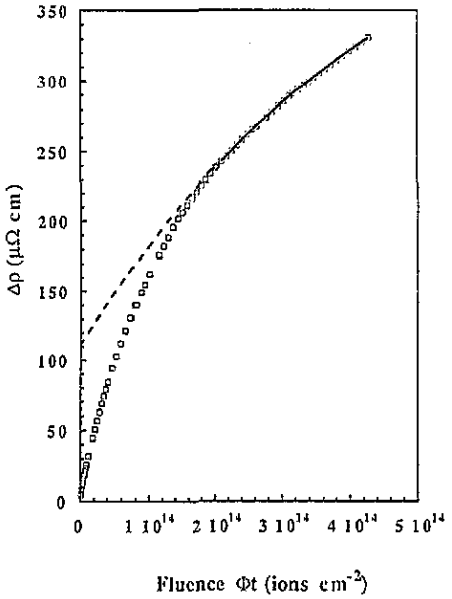

Figure 1. Resistivity increment of Bi irradiated by oxygen ions. The squares correspond to the experimental results. The line corresponds to the fit of the data in the high fluence range using (1) to determine $\Delta\rho_s = 480\ \mu\Omega$ cm and $V_0 = 190$ atomic volumes. The extrapolation to low fluence of the fit in the high fluence regime confirms the two-step processes in the damage creation in bismuth.

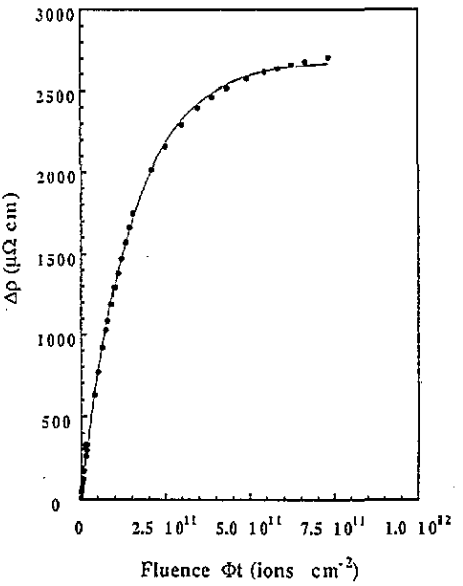

Figure 2. Same as figure 1 for lead irradiation. The line is a fit of the data using (1), leading to $\Delta\rho_s = 2690\ \mu\Omega$ cm and $\sigma_E = 5.9 \times 10^{-12}$ cm^2. Note that the saturation resistivity is reached at a very low fluence compared to figure 1.

[40], σ of (1) can be written $\sigma = 2v_0\sigma_N$ where v_0 is the number of atomic volumes where spontaneous recombination occurs, and σ_N is the nuclear collision cross section [38, 39]. In the nuclear collision regime, v_0 is close to 190 atomic volumes in agreement with electron irradiation data [32]. Moreover, an extrapolation of the data in figure 1 according to (1) indicates a saturation resistivity of the order of 480 $\mu\Omega$ cm as is the case for electron irradiation [32].

In the electronic regime, good agreement between (1) and experimental data is obtained irrespective of irradiation fluence, as demonstrated in figure 2. The resistivity increment at saturation $\Delta\rho_s$ is equal to 2690 $\mu\Omega$ cm (see table 2). This value is five times higher than in the nuclear collision regime. Such behaviour is drastically different from that of e.g. iron [5, 41] for which the saturation resistivity decreases as S_e increases. It appears that the irradiation in the S_e regime induces drastic changes in Bi. Such changes are assumed to occur by the following process: melted zones are formed in the wake of the incoming ions and are quenched into the amorphous state. These amorphous zones should be instable against crystallization due to the irradiation temperature higher than the temperature at which the onset of crystallization takes place in thin Bi film [27, 28]. Indeed, in contrast to the case of amorphous Bi, no sign of superconductivity could be detected down to 3 K in our irradiated samples and the saturation resistivity is of the same order of magnitude as that of the high-resistivity phase obtained after crystallization of an amorphous Bi film [27, 28]. Thus the proposed process leads to the formation of transformed bismuth, and the resulting structure of the tracks could well be close to that of the high resistivity phase above

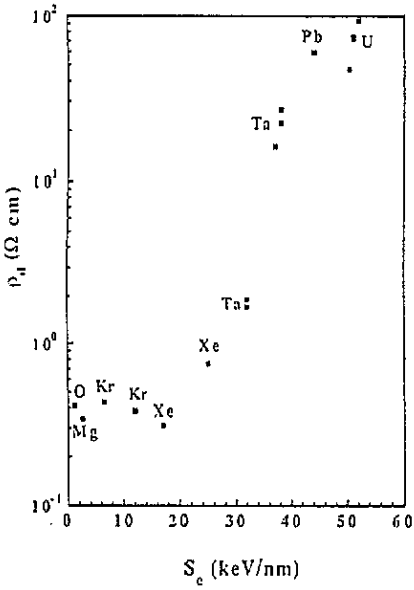

Figure 3. Initial slope of $\Delta\rho(\phi t)$ curve normalized by σ_N versus S_e. The sharp increase of ρ_d for $S_e > 24$ keV nm^{-1} indicates the creation of the high-resistivity phase of Bi by the electronic excitation.

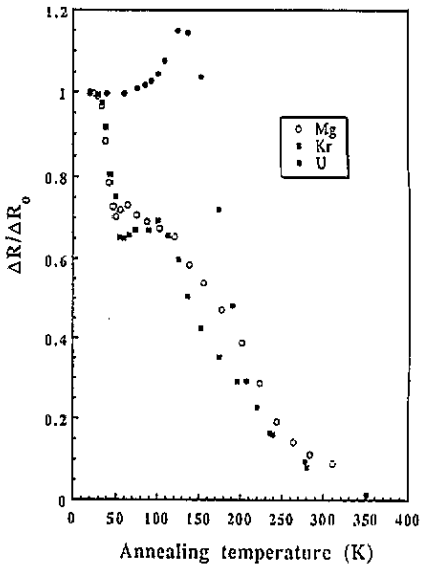

Figure 4. Isochronal annealing of Bi irradiated with Mg, Kr and U ions. ΔR_0 is the resistance increase due to the irradiation. ΔR is the resistance increase due to irradiation and annealing at temperature T. ΔR_0 and ΔR were both measured at 20 K. In the nuclear collision regime (Mg and Kr ions) the recovery stage at 45 K is clearly seen. For uranium irradiations the first stage annealing appears at 150 K.

mentioned [27, 28]. $\Delta\rho_s$ can then be regarded as the difference between the resistivities of non-irradiated and irradiated zones respectively. The parameter σ then represents the cross section area σ_E of the tracks. Assuming further a cylindrical geometry allows calculation of the tracks' radii, which can reach up to 21.9 nm for $S_e = 51$ keV nm^{-1} (see table 2). So large values have never been observed in non-radiolytic materials: neither in metals [9], in semiconductors [25] nor in insulators [42].

The threshold regime represents an intermediate case between nuclear collisions and electronic regimes respectively: both $\Delta\rho_s$ and σ_E start to increase as soon as S_e exceeds 24 keV nm^{-1}. It must be noted that while σ_E continues to increase, $\Delta\rho_s$ stays at a mean value of 2610 $\mu\Omega$ cm when S_e is higher than 30 keV nm^{-1} (table 2).

As emphasized above, both the damage mechanism and the nature of the irradiation-induced damage are not the same according to the value of the electronic stopping power. This point is in agreement with the isochronal annealing data presented in figure 4. In the nuclear collision regime, the annealing curves of figure 4 are in qualitative agreement with the data recorded after electron irradiation [29–33]: a well defined recovery stage regardless of the value of S_e in which about 30% of the irradiation-induced resistivity increment is recovered takes place at 45 K. This stage which can be attributed to the annealing of close Frenkel pairs is followed by a slower decrease in resistivity which is not completely recovered at room temperature.

The electronic regime gives rise to a strikingly different annealing behaviour (see figure 4). The 45 K annealing stage is no longer present and the recovery only starts

Table 2. Results in the electronic stopping power regime, i.e. for $S_e = dE/dx$ larger than 30 keV nm^{-1}. All the definitions are given in table 1 except for $\Delta\rho_s$ which is the saturation resistivity, σ_E the electronic stopping power damage cross section and R the radius, i.e. $\sigma_E = \pi R^2$.

Ion	dE/dx (keV nm^{-1})	$d\Delta\rho/d\phi t$ at $\phi t = 0$ (Ω cm^3/ions)	$\Delta\rho_s$ ($\mu\Omega$ cm)	σ_E (cm^2)	R (nm)
Ta	32	1.9×10^{-16}	‡	7.3×10^{-14}	1.5
	37	3.0×10^{-15}	‡	1.1×10^{-12}	6.0
	38	6.1×10^{-15}	‡	2.3×10^{-12}	8.5
		4.8×10^{-15}	‡	1.8×10^{-12}	7.6
Pb	44	1.6×10^{-14}	2690	5.9×10^{-12}	13.8
U	49	2.7×10^{-14}	2600	10×10^{-12}	18.2
	50	3.7×10^{-14}	2560	14×10^{-12}	21.4
		3.6×10^{-14}	2560	14×10^{-12}	21.4
	51	3.9×10^{-14}	2590	15×10^{-12}	21.9

‡ Assuming $\Delta\rho_s = 2610$ $\mu\Omega$ cm mean value of Pb and U results.

at a temperature of 150 K. Although this disappearance of the first annealing stage as S_e increases is a general behaviour of metals [4, 41, 43] sensitive to electronic excitation, the data for irradiated Bi are unusual since the 45 K annealing stage disappears completely within a very small range of S_e at the onset of the electronic regime. This behaviour can then be related to the change of the damage mechanism as a function of S_e. At low electronic slowing down, the damage almost consists in Frenkel pairs creation which recover during annealing, while at high S_e a new phase is induced by irradiation. Finally, an increase of the sample resistance during annealing can be observed in the temperature range from 50 to 130 K. Such behaviour has already been observed in irradiated Bi and attributed to a lattice disordering which takes place before vacancy migration.

4. Discussion: latent tracks radii calculations

The aim of this section is to present, in the framework of the thermal spike model, a calculation of the radii of the latent tracks assumed to be induced by swift heavy-ion irradiation in bismuth and to check the consistency of the obtained results assuming that the molten phase should initiate the observed defect creation.

When ion energy is lost in a solid by electronic slowing down, the electronic system locally undergoes a rapid heating up to a temperature T_e of the same order of magnitude as the Fermi temperature. The deposited energy is then shared between the target electrons and the lattice atoms via respectively electron–electron and electron–phonon interaction. This phenomenon can be accounted for by a set of coupled equations in cylindrical geometry:

$$\begin{aligned} C_e(T_e)\partial T_e/\partial t &= \nabla(K_e(T_e)\nabla T_e) - g(T_e - T) + A(r,t) \\ C(T)\partial T/\partial t &= \nabla(K(T)\nabla T) + g(T_e - T). \end{aligned} \tag{2}$$

C, K and T are the specific heat, the heat conductivity and the temperature respectively of the electronic system (with a subscript e) and of the lattice (with no subscript). g is the electron–phonon coupling constant. $A(r,t)$ is the energy transferred to the electrons by the incident ion at a time t and at a radial distance r from the ion wake [19]:

$$A(r,t) = bS_e \exp[-(t - t_0)^2/2\alpha^2] \exp(-r/r_0). \tag{3}$$

t_0 is the time, of the order of 10^{-15} s [20], required for the electrons to reach the equilibrium distribution. This time corresponds to the time of flight of the mean energy delta electrons. The half-width of the Gaussian distribution (α) is assumed to be equal to t_0. The rate of the exponential decay of the spatial distribution r_0 has been estimated ($\simeq 2.5$ nm) by Waligorsky *et al* [44]. Finally b is a normalization constant chosen so that $\int\int 2\pi r A(r,t)\,dr\,dt = S_e$.

All the parameters involved in the two equations are temperature dependent. Moreover, the calculations have to account for a solid to liquid phase transition so that only a numerical resolution of equations is possible [19].

In the S_e range covered in the present experiments, it can be assumed that the five valence electrons of bismuth atoms, located around the ion path in a spatial area larger than the ion track, are excited into the conduction band. In the following, the excited electron density is then $n_e = 1.42 \times 10^{23}$ electrons cm^{-3} and assuming further a rigid band model, the Fermi energy is $\epsilon_F = 9.9$ eV. The parameters C_e, K_e and g can be also calculated using the formalism of the free electron model [45]. As long as T_e is lower than the Fermi temperature, the electron heat capacity can be considered proportional to T_e: $C_e = n_e T_e \pi k^2/2\epsilon_F$. At the Fermi temperature (T_F), C_e becomes constant: $C_e = 3kn_e/2$. The electronic thermal conductivity $K_e(T_e)$ is linked to the electronic diffusivity $D_e(T_e)$ through the relation $K_e(T_e) = C_e(T_e)D_e(T_e)$. The evolution of D_e as a function of T_e has been evaluated by Martynenko and Yavlinskii [24]. In noble metals which are relatively well described by the free electron gas model, there is only a qualitative agreement between the theoretical predictions and the data. The difference comes from the fact that the free electron gas model does not take into account the crystal structure, the electron–phonon interaction and the electron–electron interaction. Hence a precise prediction of $D_e(T_e)$ is not possible. To overcome this we have assumed that $D_e(T_e)$ will follow the predicted evolution [24] scaled by measurements of the conductivity $\sigma_e(T_e)$ of a noble metal (gold) at 20 K (equal to the irradiation temperature). From [36], $\sigma_e(20\text{ K}) = 10^8\ \Omega^{-1}\ \text{cm}^{-1}$ leading to $D_e(20\text{ K}) = 3.8 \times 10^4$ cm^2 s^{-1} [45]. This experimental scaling is used to take into account the interactions neglected in the free electron gas model. Hence $D_e(T_e)$ can be approximated by a T_e^{-2} law up to 300 K, followed by a T_e^{-1} law until $D_e(T_e)$ reaches its minimum value (called D_m) depending on the electron density [24]. The determination of $D_e(T_e)$ at higher temperature can be neglected. For bismuth $D_m = 4$ cm^2 s^{-1}. The D_e determination will be discussed later on in the light of the results of the track radii calculations.

The electron–phonon coupling constant g is the key parameter governing the rate of the electron energy relaxation towards the lattice. When the temperature of the electronic system is higher than the Debye temperature, the free electron model yields [22, 23]

$$g = (\pi^2/6)m_e n_e v^2/\tau(T_e)T_e \qquad \text{for} \qquad T_e \gg T_D \tag{4}$$

where v is the sound velocity and T_D the Debye lattice temperature. The sound velocity $v = kT_D/\hbar(6\pi^2 n_a)^{1/3}$ where n_a is the atomic density and k is the Boltzmann constant. $\tau(T_e)$ is the electron mean free time between collisions at temperature T_e and is related to the electronic conductivity [45] of the irradiated metal. For $T_e > T_D$

$$g = \frac{\pi^4}{18}\frac{1}{(6\pi^2)^{2/3}}\frac{1}{(n_a)^{2/3}}\frac{(n_e e T_D)^2}{L\sigma_e(T_e)T_e} \tag{5}$$

where $L = (\pi^2/3)(k/e^2)$ is the Lorentz number and e the electronic charge.

Table 3 compares g values calculated at the temperature $T_e = 273$ K with data derived from femtosecond pulse laser irradiation experiments of several metals [14, 15]. Except in the case of Nb, equation (5) provides g values higher, by a factor of one to four, than the experimental data. On the other hand, g can be evaluated assuming the Wiedemann–Franz law is valid ($K(T_e) = L\sigma_c(T_e)T$) which yields, for bismuth, g values lower by a factor of ten than in table 3. Taking into account all these considerations, g could range from 1 to 60×10^{11} W K^{-1} cm^{-3}. Since an accurate determination of g is not possible, g will be considered as a free parameter, independent of T_e since $\tau(T_e)$ follows a T_e^{-1} law. It is observed that, in the present formalism, $D_e(T_e)$ only describes the energy diffusion in the electron subsystem while g accounts more specifically for the electronic properties of the irradiated metal [11]. The values of the thermodynamic parameters involved in (2) are given in table 4.

Table 3. Theoretical determinations of the electron–phonon coupling g: comparison with the experimental values for different metals [14–16]. σ_c(273 K) is the electrical conductivity at 273 K, T_D is the Debye temperature, and n_e is the electron density.

Metals	σ_c(273 K) (10^3 Ω^{-1} cm^{-1})	T_D (K)	n_e (10^{22} e cm^{-3})	g calculated 10^{10} J K^{-1} cm^{-3} s^{-1}	g measured 10^{10} J K^{-1} cm^{-3} s^{-1}
Cu	645	315	8.5	9.7	4.8
Ag	680	215	5.9	2.6	2.8
Au	498	170	5.9	2.2	2.8
Cr	83	460	8.3	156	42
W	208	310	12.6	77	26
V	55	390	14.1	560	523
Nb	74	275	11.1	142	387
Ti	26	380	11.3	809	185
Pb	59	88	13.2	42	12
Bi	9.5	120	14.2	560	§

§ not measured by femtosecond laser experiments.

Table 4. Lattice thermal parameters.

Thermal conductivity (W K^{-1} cm^{-1})	Solid	$T < 110$ K	$K = 16.3\ T^{-1}$
		$T > 110$ K	$K = 1.55\ T^{-0.5}$
	Liquid		$K = 0.17$
Specific heat (J g^{-1} K^{-1})	Solid	$T < 50$ K	$C = 3.3 \times 10^{-3}\ T - 4 \times 10^{-3}$
		$T > 50$ K	$C = 9.6 \times 10^{-5}\ T + 9.2 \times 10^{-2}$
	Liquid		$C = 0.15$
Melting temperature: $T_m = 544$ K			
Latent heat of fusion: 54 J g^{-1}			
Specific mass	Solid 9.81 g cm^{-3}		
	Liquid 10.02 g cm^{-3}		

The latent tracks radii, deduced from the cross sections reported in table 2, are plotted in figure 5 as a function of S_e. The solid lines in this figure correspond to g values ranging from 3 to 8×10^{11} W K^{-1} cm^{-3}. These g values are in good agreement with the above

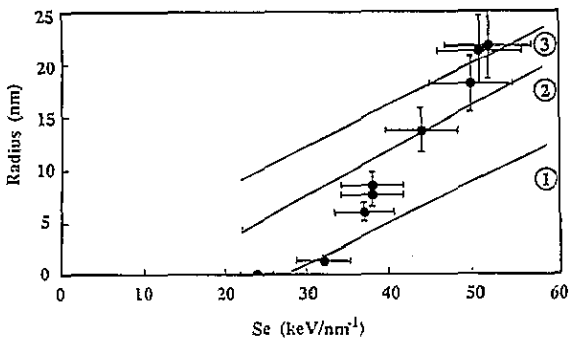

Figure 5. Latent tracks radii versus S_e. The error bars correspond to 10% for S_e and 15% for the radii. The lines correspond to the radii of the melted cylinders as calculated by the thermal spike model for different values of g and S_e. The curves labelled 1, 2 and 3 correspond to g values equal to 3, 5 and 8×10^{11} W K^{-1} cm^{-3} respectively.

estimations. Taking into account the number of parameters which is used in the present calculations the results of the calculation are in good agreement with the experiment.

The calculation results depend on the initial conditions of the input parameters. $D_e(20\,K)$ is the crucial one: increasing it by a factor of ten allows us to predict the experimental points with g values ranging between 2 and 6×10^{12} W K^{-1} cm^{-3}. Even if we strictly used the predicted evolution of $D_e(D_e(20\,K) = 6 \times 10^6$ cm^2 s^{-1} [24] and T_e^{-2} law up to $D_m = 4$ cm^2 s^{-1}) with $S_e = 50$ keV nm^{-1}, g should be less than 10^{12} W K^{-1} cm^{-3} to exclude melting in a cylinder of 1 nm. Therefore unrealistic values of D_e had to be used in order to avoid melting of Bi in the expected g range values.

5. Conclusions

Due to its peculiar physical properties, bismuth was thought to be a good candidate to ascertain whether the thermal spike phenomenon is able to account for irradiation damage in the electronic stopping power range. Polycrystalline bismuth ribbons were irradiated at 20 K with swift heavy ions from ^{18}O to ^{238}U in the GeV range. Above a S_e threshold of 24 keV nm^{-1}, a damage induced by electronic slowing down was clearly evidenced. Such a threshold value is lower than previously reported for other crystalline metals or alloys. Above 30 keV nm^{-1}, the electronic slowing down was efficient enough to induce large latent tracks up to a diameter of 43.8 nm for $S_e = 51$ keV nm^{-1} which is the largest value reported so far for non-radiolytic materials. In the S_e range higher than 30 keV nm^{-1}, the irradiation induced a high resistivity phase probably linked to the crystallization of the amorphous latent tracks. As all these features demonstrated the expected sensitivity of bismuth against electronic slowing down, latent tracks radii calculations based on the thermal spike model were developed. Assuming a realistic value for the electron–phonon coupling constant ($g = 3$ to 8×10^{11} W K^{-1} cm^{-3}) it was possible to account reasonably well for the data. A good agreement was also obtained previously in the case of amorphous alloys [17–20] which supported the idea that the thermal spike model could account, at least in part, for the observed radiation damage. In this calculation, according to g determination, metals with a high electron density, high Debye temperature and low electrical conductivity would be good candidates for the investigation of damage creation by high electronic excitation.

Acknowledgments

The authors are grateful to M N Metzner for the sample preparation and mounting. One of the authors (CD) is supported by Commissariat à l'Energie Atomique and Région de Basse Normandie.

References

[1] Fleisher R L, Price P B and Walker R M 1975 *Nuclear Tracks in Solids: Principles and Applications* (Berkeley: California University Press)
[2] Ming-dong Hou, Klaumunzer S and Schumacher G 1990 *Phys. Rev.* B **41** 1144
[3] Audouard A, Balanzat E, Fuchs G, Jousset J C, Lesueur D and Thomé L 1987 *Europhys. Lett.* **3** 327
[4] Iwase A, Sasaki S, Iwata T and Nihira T 1987 *Phys. Rev. Lett.* **58** 2450
[5] Dunlop A, Lesueur D, Morillo J, Dural J, Spohr R and Vetter J 1989 *C. R. Acad. Sci., Paris* **309** 1277; 1990 *Nucl. Instrum. Methods* B **48** 419
[6] Audouard A, Balanzat E, Jousset J C, Chamberod A, Fuchs G, Lesueur D and Thomé L 1991 *Phil. Mag.* B **63** 727
[7] Dunlop A, Legrand P, Lesueur D, Lorenzelli N, Morillo J, Barbu A and Bouffard S 1991 *Europhys. Lett.* **15** 765
[8] Paumier E, Toulemonde M, Dural J, Rullier-Albenque F, Girard J P and Bogdanski P 1989 *Europhys. Lett.* **10** 555
[9] Barbu A, Dunlop A, Lesueur D and Averback R S 1991 *Europhys. Lett.* **15** 765
[10] Desauer F 1923 *Z. Phys.* **12** 38
[11] Seitz F and Koehler J S 1956 *Solid State Phys.* **2** 305
[12] Lifshitz I M, Kaganov M I and Tanatarov L V 1960 *J. Nucl. Energ.* A **12** 69
[13] Fleisher R L, Price P B and Walker R M 1965 *J. Appl. Phys.* **36** 3645
[14] Groeneveld R H M, Sprick R and Lagendijk A 1992 *Phys. Rev.* B **45** 5079
[15] Brorson S D, Kazeroonian A, Moodera J S, Ippen E P, Dresselhaus M S and Dresselhaus G 1990 *Phys. Rev. Lett.* **64** 2172
[16] Qiu T Q and Tien C L 1992 *Int. J. Heat Mass Transfer* **35** 719
[17] Toulemonde M, Dufour C and Paumier E 1992 *Phys. Rev.* B **46** 14 362
[18] Toulemonde M, Paumier E and Dufour C 1993 *Radiat. Eff. Defects Solids* **126** 201
[19] Dufour C, Lesellier de Chezelles E, Delignon V, Toulemonde M and Paumier E 1992 *Modifications Induced by Irradiation in Glasses* ed P Massoldi (Amsterdam: North-Holland) p 61
[20] Dufour C, Paumier E and Toulemonde M 1993 *Rad. Eff. Defects Solids* **126** 119
[21] Szenes G 1992 *Mater. Sci. Forum* **97–9** 647
[22] Kaganov M I, Lifshitz I M and Tanatarov L V 1957 *Sov. Phys.–JETP* **4** 173
[23] Allen P B 1987 *Phys. Rev. Lett.* **59** 1460
[24] Martynenko Yu V and Yavlinskii Yu N 1983 *Sov. Phys.-Dokl* **28** 391
[25] Izui K and Furuno S 1986 *Proc. XIth Int. Congr. on Electron. Microscopy (Kyoto, 1986)* ed T Imura, S Maruse and T Suzuki (Tokyo: Japanese Society of Electron Microscopy) p 1299
[26] Audouard A, Balanzat E, Fuchs G, Jousset J C, Lesueur D and Thomé L 1992 *Mater. Sci. Forum* **97–9** 631
[27] Buckel W and Hilsch R 1954 *Z. Phys.* **138** 109
[28] Hamada T, Yamakawa K and Fujita F E 1981 *J. Phys. F: Met. Phys.* **11** 657
[29] Le Goff M 1984 *CEA report* R-5288
[30] Bois P and Beuneu F 1987 *J. Phys. F: Met. Phys.* **17** 2365
[31] Bois P and Beuneu F 1989 *J. Phys.: Condens. Matter* **1** 4535
[32] Beuneu F and Bois P 1988 *Phys. Rev.* B **37** 6041
[33] Bois P 1987 *CEA report* R-5389
[34] Meyer E and Linderer L 1976 *J. Low Temp. Phys.* **22** 517
[35] Quelard G 1978 *CEA Report* R-4866
[36] Meaden G T 1965 *Electrical Resistance of Metals* (London: Plenum)
[37] Bouffard S, Dural J, Levesque F and Ramillon J M 1989 *Ann. Phys., Paris* **14** 395
[38] Biersack J P TRIM91 [39]
[39] Biersack J P and Haggmark L G 1980 *Nucl. Instrum. Methods* **174** 257
[40] Wollenberger H J 1969 *Vacancies and Interstitials in Metals* (Amsterdam: North-Holland)

[41] Legrand P, Dunlop A, Lesueur D, Lorenzelli N, Morillo J and Bouffard S 1992 *Mater. Sci. Forum* **97–9** 587
[42] Hansen P, Hertmann H and Smit P M 1982 *Phys. Rev.* B **26** 3539
[43] Iwase A, Sasaki S, Iwata T and Nihira T 1985 *J. Nucl. Mater.* **133–4** 365
[44] Waligorski M R P, Hamm R N and Katz R 1986 *Nucl. Tracks Meas.* **11** 309
[45] Ashcroft N W and Mermin N D 1976 *Solid State Physics* (New York: Holt, Reinhart and Winston)